Available online at www.sciencedirect.com
SCIENCE DIRECT®
Journal of Nuclear Materials 337–339 (2005) 737–741
journal of nuclear materials
www.elsevier.com/locate/jnucmat

Direct measurement of the impurity dynamics during an ELM cycle

M.R. Wade [a,*], K.H. Burrell [b], J.T. Hogan [a], A.W. Leonard [b], T.H. Osborne [b], P. Snyder [b], D. Coster [c]

[a] *Oak Ridge National Laboratory, Oak Ridge, TN 37831, USA*
[b] *General Atomics, P.O. Box 85608, San Diego, CA 92186-5608, USA*
[c] *Institute for Plasma Physics, Garching, Germany*

Abstract

Using high spatial and temporal resolution spectroscopy, the first direct measurements of the impurity dynamics during an ELM cycle have been made in the DIII-D tokamak. These measurements confirm that significant impurity density is expelled by each ELM with the degree of expulsion dependent on the ELM size. The observed perturbation to the impurity density profile is comparable to that of the electron density, suggesting that all particle species are similarly affected by the ELM. Impurity confinement in the edge is observed to improve throughout the phase between ELMs and is associated with a continuous increase in the $E \times B$ shear near the edge.

PACS: 52.25.Vy; 52.55.Fa; 52.30.Cv; 52.55.Tn
Keywords: DIII-D; Edge plasma; ELM; Impurity transport

1. Introduction

For many years, it has been well established that edge localized modes (ELMs) in tokamak plasmas play an important role in controlling the impurity content of the confined plasma [1]. In particular, ELM-free H-mode plasmas have been shown to suffer unabated accumulation of both low-Z and high-Z impurities [2,3]. In contrast, H-mode plasmas with frequent ELMs generally have relatively low impurity contamination. However, due to the lack of adequately resolved (both in time and space) measurements of the impurity dynamics associated with an ELM, the exact details of the ELM expulsion process are still not well known. Recent upgrades in the DIII-D charge-exchange recombination (CER) spectroscopy system [4] have made possible the measurement of the impurity dynamics during the ELM cycle with unprecedented spatial and temporal resolution. Taking advantage of this capability, measurements have been made of the impurity response to the ELM event and subsequent refueling of the core plasma. These measurements indicate a rapid decrease in the density of fully stripped carbon (n_{C+6}) in the edge region at each ELM that is dependent on the magnitude of the ELM energy loss. Coincident with this decrease, an increase of n_{C+6} in the scrape-off layer (SOL) region is observed,

* Corresponding author. Address: General Atomics, P.O. Box 85608, San Diego, CA 92186-5608, USA. Tel.: +1 858 455 4165; fax: +1 858 455 4156/3492.
E-mail address: wade@fusion.gat.com (M.R. Wade).

0022-3115/$ - see front matter © 2004 Elsevier B.V. All rights reserved.
doi:10.1016/j.jnucmat.2004.10.121

confirming the role of ELMs in expelling impurities from the confined region of ELMing H-mode plasmas.

ELM studies have intensified in recent years as the International Thermonuclear Experimental Reactor (ITER) design process and associated physics basis has identified the type I ELMing H-mode regime as the reference operating mode for ITER [5]. New experimental and theoretical capabilities have been brought to bear on the study of ELMs aimed at developing a sufficient knowledge base such that one can maximize the beneficial effect of ELMs (e.g., impurity removal) while minimizing the unfavorable aspects (e.g., high transient heat and particle fluxes on plasma facing surfaces). While the characterization is still far from complete, these studies suggests that Type I ELMs are ideal, magnetohydrodynamic (MHD) moderate n (~5 to 20) instabilities originating near the plasma edge that have limited radial extent [6]. However, this inference is primarily based on the response of the electrons, as measurements of the ion and impurity response have lacked sufficient temporal or spatial resolution. Soft X-ray measurements on Alcator C-Mod [7] have shown that impurities are expelled from the edge by each ELM, but due to the line-integral nature of the measurement and the measurement dependence on the electron density and temperature, details of the expulsion process are difficult to unambiguously determine. In addition, no information is available on the impurity temperature or rotation response.

2. Experimental results

Taking advantage of recent upgrades to the DIII-D CER system to allow sub-millisecond data framing, the evolution of the impurity density, temperature, and rotation have been measured during the ELM cycle and have revealed several details not previously observable. This system consists of 40 channels that view across three separate neutral beams. The spatial resolution for impurity density and ion temperature (T_i) measurement is ~3 cm in the core plasma and ~3 mm in the edge plasma, while the resolution for toroidal and poloidal rotation (v_{tor} and v_{pol}) measurement is ~6 cm in the core and ~6 mm in the edge. The resolution in the edge is sufficient to provide detailed information on the profiles in the high gradient region near the edge of an H-mode plasma. Recently, this system has been upgraded to allow excellent signal-to-noise detection at high time resolution, allowing accurate determination of the spectral features (namely brightness, Doppler width, and Doppler shift) of the detected CER spectra at acquisition rates never before possible. Data framing times as low as 274 μs have been used successfully. The majority of the data used for this study was taken with 550 μs framing times. In the cases discussed here, the C VI $n = 8$–7 transition at 5290 A is used. This provides a direct measurement of the density, temperature, and rotation velocity of C + 6 in the edge plasma.

An example of the quality of data available from this system is shown in Fig. 1 where the temporal evolution of n_{C+6}, T_i, v_{tor} and v_{pol} deduced by CER spectroscopy for several radial locations during a series of ELM events is shown. Main plasma parameters for this discharge are $I_p = 1.3$ MA, $B_t = -1.75$ T, $P_{inj} = 4.3$ MW, $f_{ELM} = 20$ Hz and $n_e = 8 \times 10^{19}$ m^{-3} (no external gas fueling) in a lower single null configuration. From Fig. 1, it is clear that each ELM causes a significant decrease in n_{C+6} on a very short time scale over a limited spatial region localized near the plasma edge. For each of the channels in the radial region 2.2 m < R < 2.285 m, a rapid drop in the impurity density is observed coincident with the ELM event. Note that the time for the data shown in Fig. 1 represents the central time for the integration period. The decrease in the case shown in Fig. 1 occurs in no more than one integration period (550 μs), and possibly less. At the fastest time resolution available to date of 3.7 kHz (270 μs integration time), the expulsion is also observed to occur in less than one integration period, indicating the expulsion occurs in less than 300 μs. Coincident with this rapid decrease in the edge plasma is a rapid increase in n_{C+6} in the midplane

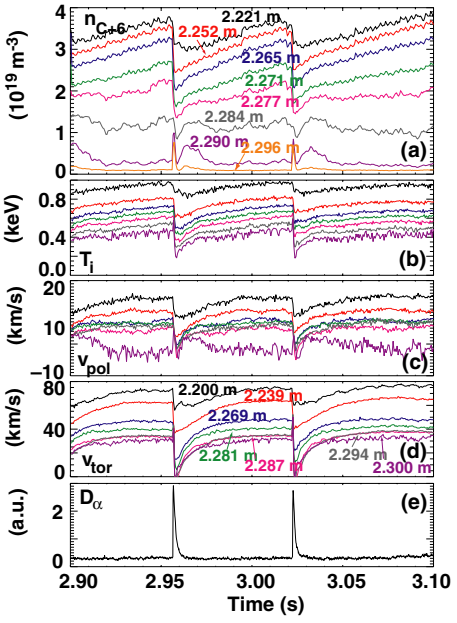

Fig. 1. Temporal evolution of edge impurity profiles during a set of ELM cycles: (a) fully stripped carbon density; (b) impurity/ion temperature; (c) poloidal rotation; (d) toroidal rotation at various radial locations along the outboard midplane and (e) midplane D_α signal. Color scheme is the same for (a), (b), and (c). For (c) and (d), SOL data is not included. In this case, the separatrix location is $R_{sep} = 2.29$ m.

SOL ($R > 2.285$ m). Detailed analysis (using cases with and without active CER emission) indicates that this increase is almost entirely due to an increase in beam-induced CER emission with only a small increase in background emission due to thermal charge-exchange or electron impact excitation.

The relative perturbation to the n_{C+6} and electron density n_e profiles from measurements taken just before and after a series of reproducible ELMs is shown in Fig. 2. The CER data framing rate in this case is such that the data is taken within ±0.55 ms of the ELM. Due to the lower time resolution of the Thomson scattering measurements, the n_e perturbation is deduced using the method described in Refs. [8,9]. The excellent spatial resolution for n_{C+6} is made possible by a radial sweep of the outboard separatrix location during several reproducible ELMs. From Fig. 2, it is evident that the impurity density decreases across the region $0.6 < \hat{\rho} < 0.97$ with the maximum decrease occurring near $\hat{\rho} = 0.92$. Inside $\hat{\rho} = 0.6$, the effect of the ELM is negligible. Also evident from Fig. 2 is that the perturbation to n_{C+6} is almost identical to that of n_e with both perturbations near 40% of the original density at $\hat{\rho} = 0.92$. Over the limited data set obtained to date, the radial structure of the perturbation in n_{C+6} is rather insensitive to the ELM energy loss while the magnitude of the perturbation is observed to increase with the ELM energy loss (see Fig. 3). The similarity of the n_{C+6} and n_e perturbations suggests also that the main ion perturbation will also be quite similar due to quasi-neutrality constraints. This suggests that the convective portion of the energy loss due to the ELM may arise from electrostatic turbulence since $E \times B$ transport should not be species dependent.

Coincident with the rapid decrease in the edge region, the n_{C+6} in the SOL is observed to increase dramatically (see Fig. 3). This increase appears to have significant radial extent, extending at least 10 cm beyond the separatrix. The characteristic e-folding length of the perturbation in the SOL is on the order of 10 cm, which suggests that the perturbation may extend all the way to the wall on the outboard midplane. This observation is similar to the observed electron density response [10]. As shown in the table accompanying Fig. 3, the majority of the impurity energy transport associated with the

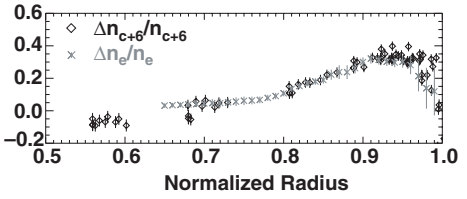

Fig. 2. Comparison of the relative density decrease caused by an ELM to n_{C+6} (black) and n_e (grey) profiles versus normalized radius.

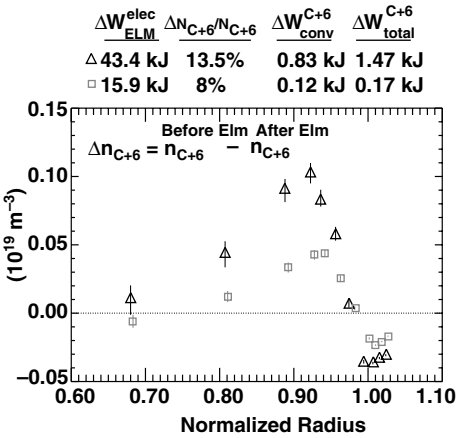

Fig. 3. Measured perturbation to the n_{C+6} density for ELMs of two different sizes (denoted by black and grey) along with tabulated values of perturbation amplitude: ΔW^{elec}_{total} is the electron energy loss; $\Delta n_{C+6}/n_{C+6}$ is the fractional carbon inventory loss; ΔW^{C+6}_{conv}, and ΔW^{C+6}_{total} are impurity, convective, and total energy losses, respectively. The larger ELM is from the same discharge as that of Figs. 1 and 2.

ELM is convective in nature. The impurity convective and conductive energy losses are defined as $\Delta W_{conv} = 3/2\int\langle T_i\rangle\Delta n_{C+6}\,dV$ and $\Delta W_{cond} = 3/2\int\langle n_{C+6}\rangle\Delta T_i\,dV$, respectively. Here, $\langle x\rangle$ indicates an average between the pre-ELM and post-ELM values, Δx indicates the change between the pre-ELM and post-ELM values, and the integral is plasma volume. The two cases in Fig. 3 are identical except for the use of strong gas fuelling in the small ELM case, leading to a density roughly 30% higher. In both cases in Fig. 3, ΔW_{conv} accounts for more than 50% of the total impurity energy loss. As seen before in studies of the electron response, the convective loss fraction increases as the density increases. However, it should be noted that the plasma density in these two cases is in a range ($n_{e,ped}/n_{GW} = 0.5$–0.65) which represents the upper end of previously reported results on the electron response. Because of this, it is difficult to compare the observed perturbations here with that obtained in previous DIII-D studies of the electron response to the ELM.

There is evidence from a comparison of response of the tangential and vertically viewing systems that the ELM expulsion process occurs in a poloidally localized region near the outboard midplane. This data is shown in Fig. 4. The CER beams are turned off in this case; hence, the intensity in Fig. 4 is the line-integral of electron excitation emission from C + 5 viewed by each CER channel. The signal observed during the ELM is a factor of 100 larger than that observed between ELMs. Spectral analysis indicates a nearly constant ion temperature of ~1 keV for all viewing chords during the ELM, implying that the observed spectral emission originates

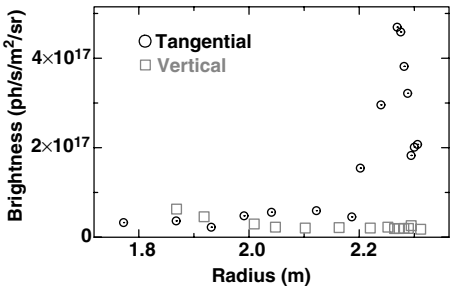

Fig. 4. Measured spectral brightness versus CER viewing location [tangency radius for tangentially viewing chords (circles), radial position at midplane for vertically viewing chords (squares)] during an ELM with the CER beams turned off.

internal to the plasma. The observed radial dependence of the tangential channels in Fig. 4 is consistent with that expected in the presence of a radially localized emitting shell of limited radial extent. CER channels with views tangent to this emitting shell should measure the largest signal, suggesting a peak in emission near $R = 2.28$ m. This interpretation of the tangential data is consistent with calculations based on the plasma equilibrium and CER system viewing geometry and assuming an emitting shell extending from $0.9 < \hat{\rho} < 1$. However, the lack of a response on the vertically viewing chords is inconsistent with a poloidally symmetric emitting shell in this region. Estimates indicate that the emitting shell must be limited to $< \pm 3$ cm of the outboard midplane to explain the vertical channel data in Fig. 4. Simulations of the non-linear phase of the ELM instability do suggest the formation of helical structures that have significantly more toroidal extent than poloidal. More work (including time-dependent transport studies) is necessary to assess whether the degree of poloidal localization observed in these measurements is consistent with these simulations.

Subsequent to the ELM event, n_{C+6} in the SOL rapidly drops back near its pre-ELM level and then begins to increase. This second increase in the SOL lasts for approximately 10 ms and appears to be uniform in temporal response across the entire SOL measurement region. Note that n_{C+6} in the edge plasma during this time does increase but not nearly as much as that in the SOL. After this second increase in n_{C+6} in the SOL, there appears to be a change in the transport properties as the edge n_{C+6} continues to increase while the SOL n_{C+6} begins to decrease. This bifurcation occurs very close to the separatrix and a general increase in the edge density gradient is observed until the next ELM event. The timing of this bifurcation is correlated with a bifurcation in poloidal rotation velocities in the same region (see Fig. 1(c)) and the initial development of the E_r well near the separatrix, suggesting that the E_r well plays a role in the observed improvement in edge transport.

Taken altogether, these observations suggest that the ELM expulsion/refueling process is as follows. At the ELM event, n_{C+6} is transported radially outward from the edge plasma to the SOL. The n_{C+6} is then transported rapidly out of the SOL by parallel conduction along the open field lines to the divertor target. This pulse of particle flux at the divertor target causes increased recycling throughout the divertor, fueling the divertor SOL fairly uniformly. The recycled impurity density is then transported back towards the core region, resulting in a brief increase in the midplane SOL impurity density. Once this recycling source has diminished, the impurity density in the SOL is depleted through radial transport into the core. The edge impurity density profile then continues to steepen slowly throughout the intra-ELM phase as impurity confinement continues to improve in this region.

As an initial step in understanding the observed impurity transport behavior, a preliminary comparison of models for ELM transient behavior of C impurity density in DIII-D LSN discharges has been carried out using the solps (b2-EIRENE) scrape-off layer transport code [11]. The solps code implicitly couples a 2-D, time-dependent description of the edge/SOL plasma for all ion species of D and C, with the EIRENE 2-D neutrals transport code. Using this code, various assumptions regarding the transport enhancement induced by the ELM have been examined by enhancing separately the edge/pedestal transport, SOL transport and then both together. This choice of assumptions is motivated by the present ITER impurity transport model [12], which describes the ELM event as a simultaneous enhancement of particle and thermal transport throughout both the edge/pedestal and the SOL regions for 100–300 μs. We have examined the model sensitivity to this assumption, enhancing separately edge/pedestal transport ('gradient'), SOL transport ('SOL') and then both together ('standard'). The resulting behavior in the midplane region is qualitatively similar for all these assumptions: each of the models produces a reduction of n_{C+6} in the edge/pedestal region with a subsequent increase in SOL density and thus core refueling, due to increased C generation at the target plates. However, there are significant differences in the expected divertor behavior, which was not available for these discharges. To resolve these differences, simultaneous measurements of the core n_{C+6} and spectroscopic imaging of the ELM pulse in the divertor region are required.

3. Summary

In summary, measurements of the impurity dynamics during an ELM cycle, made possible by unprecedented time and space resolved measurements via CER spectroscopy of the edge plasma in DIII-D, have revealed

several interesting features of the impurity transport. At each ELM, a rapid (<300 μs) expulsion of impurity density from the edge plasma is observed, which extends as far in as $\hat{\rho} = 0.7$ with the peak reduction occurring at $\hat{\rho} = 0.92$. The magnitude of this perturbation increases as the ELM size increases. The impurity density in the SOL is observed to increase at the same time with the increase extending outward as far as measurements are available. The perturbation in the impurity density caused by the ELM is observed to be almost identical to that in electron density. This suggests (due to quasi-neutrality constraints) that the main ion perturbation is also similar and that the convective energy loss mechanism associated with the ELM does not depend on the particle species. More work is necessary to verify this observation over a wider range of plasma conditions.

Acknowledgments

This work was supported in part by the US Department of Energy under DE-FC02-04ER54698 and DE-AC05-00OR22725.

References

[1] H. Zohm, Plasma Phys. Control. Fusion 38 (1996) 1213.
[2] M.E. Perry et al., Nucl. Fusion 31 (1991) 1859.
[3] M.R. Wade et al., Proceedings of 23rd European Conference on Controlled Fusion and Plasma Physics, vol. 20C, Part I, European Physical Society, 1997, p. 203.
[4] K.H. Burrell et al., Rev. Sci. Instrum., submitted for publication.
[5] ITER Physics Basis, Nucl. Fusion 39 (1999) 2251.
[6] P.B. Snyder et al., Phys. Plasmas 9 (2002) 2037.
[7] J.A. Snipes et al., Plasma Phys. Control. Fusion 40 (1998) 765.
[8] G.D. Porter et al., Phys. Plasmas 8 (2001) 5140.
[9] A.W. Leonard et al., Phys. Plasmas 10 (2003) 1765.
[10] L. Zeng et al., in: 16th International Conference on Plasma Surface Interactions in Controlled Fusion Devices, 2004, Portland, Maine.
[11] R. Schneider et al., Contrib. Plasma Phys. 40 (3&4) (2000) 328;
D. Reiter, J. Nucl. Mater. 196–198 (1992) 80.
[12] A. Loarte et al., in: Proceedings of 18th IAEA Fusion Energy Conference, 2000, Sorrento, Italy, International Atomic Energy Agency, Vienna, 2001.